Tectonophysics 723 (2018) 162–171

Contents lists available at ScienceDirect

Tectonophysics

journal homepage: www.elsevier.com/locate/tecto

A restricted Linked Stress Release Model (LSRM) for the Corinth gulf (Greece)

Ourania Mangira[a,*], Rodolfo Console[b], Eleftheria Papadimitriou[a], Georgios Vasiliadis[c]

[a] Geophysics Department, School of Geology, Aristotle University of Thessaloniki, GR54124 Thessaloniki, Greece
[b] Center of integrated Geomorphology for the Mediterranean Area, Potenza, Italy
[c] Department of Informatics Engineering, TEI of West Macedonia, GR52100 Kastoria, Greece

ARTICLE INFO

Keywords:
Linked stress release model
Synthetic catalogs
Corinth gulf (Greece)

ABSTRACT

The earthquake occurrence in the Corinth Gulf (Greece) is modeled by means of the Linked Stress Release Model, which combines the gradual increase of the strain energy due to continuous tectonic loading and its sudden release when an event occurs. The modeling is based on the theory of stochastic point processes and it is determined by the conditional intensity function. The modeled time–dependent seismicity incorporates stress transfer and interactions among the major fault segments that belong either to the western or to the eastern part of the study area. Static stress changes caused by the coseismic slip of eight characteristic events that occurred during the instrumental era were calculated. Their perturbations reveal that earthquakes occurring in the eastern part provoke excitation in the western part while the events that occurred in the western part do not affect the seismicity of the eastern part. This result was taken into account and the values of the model parameters were constrained accordingly. The analysis is also performed on synthetic earthquake catalogs developed by an earthquake simulator algorithm that can replicate the seismic activity in the study area and yields to comparable results.

1. Introduction

The formulation of stochastic models for seismic hazard assessment has blossomed during the last several decades in an attempt to bridge the gap between physical and statistical models (Vere-Jones et al., 2005). The application of such models aims to improve our understanding of the evolution of the seismic activity and the associated underlying mechanisms. A connection between seismicity and physics is achieved by means of fault interaction. It is widely accepted that strong earthquakes may trigger others on nearby faults, thus altering the occurrence probability of the next event on a particular fault or fault segment. This means that the recurrence time of earthquakes on a fault is not regular and depends not only on the stress and the properties of the fault itself but also on earthquakes occurring on adjacent faults (Stein, 1999). Stress transfer and earthquake triggering have been the subject of many studies (e.g. Stein et al., 1997; King and Cocco, 2001; Steacy et al., 2005; Cocco and Rice, 2002; among others). Considerable efforts have also been exerted for stress triggering to be incorporated in seismic hazard assessment by developing methods that translate static stress changes into earthquake probability changes (Hardebeck, 2004; Parsons, 2005; Gomberg et al., 2005).

Stress transfer between adjacent areas is taken into account, from a different point of view, by means of the Stress Release Model (SRM). It is worth to be mentioned at this point that stress cannot actually be released; it can be relieved and transferred. Since this phrase is mostly used in the literature, we will also adopt it, keeping in mind though that, strictly speaking, it is an inaccurate expression.

In the Stress Release Model, introduced by Vere-Jones (1978), the energy released during an earthquake results in a period of quiescence until the re–accumulation of the energy and the genesis of the next earthquake. Interactions between different parts of an area are incorporated in the model allowing either damping or excitation of adjacent subareas due to stress transfer. The model has been successfully applied to many areas worldwide, like China (Liu et al., 1999), Taiwan (Bebbington and Harte, 2001), New Zealand (Lu and Vere-Jones, 2000), Japan (Lu et al., 1999), Romania (Imoto and Hurukawa, 2006), Greece (Rotondi and Varini, 2006; Votsi et al., 2011; Mangira et al., 2017) and Italy (Varini and Rotondi, 2015; Varini et al., 2016). A systematic study concerning the evaluation of the best model, the regionalization, the sensitivity to catalog errors and the optimization was performed by Bebbington and Harte (2003), whereas Kuehn et al. (2008) investigated by means of numerical simulations how coupling between different

* Corresponding author.
E-mail address: omangira@geo.auth.gr (O. Mangira).

https://doi.org/10.1016/j.tecto.2017.12.011
Received 27 July 2017; Received in revised form 11 December 2017; Accepted 17 December 2017
Available online 19 December 2017

areas affects the occurrence probability distributions.

The application of the Simple Stress Release Model (SSRM) in the Corinth Gulf was previously attempted by Rotondi and Varini (2006) in the western part of the Corinth Gulf using a dataset of 20 earthquakes with M ≥ 5.0 since 1945 by means of Bayesian methods. They pointed out the lack of sufficient data for getting reliable results. Mangira et al. (2017) applied the LSRM dividing the area of the Corinth Gulf into two subareas, namely to a western and an eastern part, in an attempt to investigate the kind of interactions between them. Although both transfer parameters were found positive, indicating inhibitory behavior, the value of zero (0) was included in the interval estimation of the parameter c_{12}, implying that the western part of the Corinth Gulf could be studied separately. The large positive value of the parameter c_{21} indicates relative correlation between the two subareas, and particularly earthquakes occurring in the western part provoke damping in the eastern part. Nevertheless, the loading rate in the eastern part was found high and perhaps responsible for the intense earthquake occurrence. A Weibull-type c.i.f. was also tested as an alternative to the exponential form. Although the results were quite similar, due to the fact that two extra parameters were required for the proposed model, the Akaike Information Criterion (AIC) used for evaluating the competing models, favored the use of the exponential form.

The aim of this study is to apply the LSRM in the same area again being divided in two subareas, the western and eastern part. The area is revisited in an attempt to incorporate into the model information provided from the calculation of Coulomb stress changes due to the coseismic slip of the strongest earthquakes during the study period. The kind of interactions between the two subareas is initially inspected by means of the calculations of static stress changes due to the coseismic slip of eight earthquakes associated with certain fault segments. Synthetic catalogs were then used in order to overcome shortage of data due to limited duration of earthquake catalog. The LSRM was applied to fit simulated data for investigating its performance to a much bigger sample size and testing the potential use of a synthetic catalog that could shed more light in the estimate of the model.

2. Study area and data

The Corinth Gulf, an asymmetric half–graben with the southern footwall being uplifted (Fig. 1), has been widely studied as it constitutes one of the most active structures in Greece associated with intense crustal deformation (Roberts and Jackson, 1991; Armijo et al., 1996). Both historical and instrumental records confirm the high level of seismic activity (Papazachos and Papazachou, 2003). The sequence of three destructive earthquakes (M ≥ 6.3) in less than ten (10) days in 1981 associated with adjacent and antithetic fault segments of the eastern part of the Corinth Gulf in Alkyonides Bay, has given rise to many studies in the area (Jackson et al., 1982; Hubert et al., 1996; Hatzfeld et al., 2000). Destructive earthquakes that occurred in 1992 near Galaxidi (Hatzfeld et al., 1996) and in 1995 near Aigion (Bernard et al., 1997) have also motivated several studies.

The seismicity is mainly associated with eight major active fault segments that bound the rift to the south. The western part of the Corinth Gulf includes the Psathopyrgos, Aigion and Eliki fault segments, whereas in the eastern part the seismicity is controlled by the Offshore Akrata, Xylokastro, Offshore Perachora, Skinos and Alepochori fault segments (Fig. 1). The maximum magnitude recorded or ever reported hardly exceeds 6.8, which is probably due to the lack of continuity of the faults (Jackson and White, 1989). However, the question remains whether the discontinuities are stable and will not break, or the rupture can jump from one segment to another resulting in an earthquake of greater magnitude (Jackson and White, 1989; Hatzfeld et al., 2000).

For the application of the LSRM the division of the study area into two subareas was based on seismotectonic criteria, like fault segmentation and seismicity rate. The data used are taken from the catalogs compiled by the Geophysics Department of the Aristotle University of Thessaloniki (GD–AUTh) and based on the recordings of the Permanent Regional Seismological Network (1981). After checking the completeness of the data, the magnitude threshold is chosen to be $M_{th} = 5.2$ and the catalog comprises events from January 1st, 1911 up to December 31st, 2016 in an attempt to obtain the largest and longest possible complete dataset (Table 1). As a result, 61 events are included in the dataset, 38 of which comprised in the western (stars in Fig. 1) and 23 in the eastern part (hexagons in Fig. 1) of the study area. Fig. 2a shows earthquake magnitudes as a function of their occurrence time. We can see that there is alternation of active and relative quiescent periods as well as synchronization of the two parts indicating that interactions may exist. The frequency and the cumulative number of events versus time (in years) are shown in Fig. 2b. We may see that earthquakes in the Corinth Gulf tend to occur in clusters, but there are also periods of relative quiescence. The two green lines represent two "characteristic" cases that are accompanied by a large number of events, the M_w6.3 earthquake of 22nd April 1928 and the sequence of 1981 in the eastern part of the Corinth Gulf.

3. Calculations of coulomb stress changes

Earthquake occurrence provokes redistribution of stress in the surrounding faults, and this is the main concept of the application of the SRM. Before applying the LSRM the influence of the stress changes caused by the stronger earthquakes in the study period is investigated, to the occurrence of the next earthquakes in the data sample. Coseismic Coulomb stress changes are calculated for the earthquakes with

Fig. 1. The study area where the eight major faults bounding the southern coastline are shown along with the Kapareli antithetic fault segment. Seismicity (M ≥ 5.2) is depicted with the epicenters of earthquakes. The events that occurred in the western part are represented with red stars, whereas the ones occurred in the eastern part are represented with yellow hexagons. Their size is proportional to the earthquake's magnitude.

Table 1
The occurrence time, location and magnitude of the events included in the dataset.

	Date	Epicentral coordinates		M_w
		Lat.	Long.	
1	18 Jan 1911	38.500	22.200	5.2
2	23 Jan 1911	38.500	22.200	5.2
3	16 Mar 1911	38.200	22.000	5.4
4	21 Nov 1915	38.400	21.800	5.3
5	24 Dec 1917	38.400	21.700	6.0
6	27 Dec 1917	38.400	21.800	5.3
7	27 Jan 1918	38.500	22.000	5.5
8	11 Jul 1918	38.400	21.400	5.4
9	6 Jun 1925	38.200	21.700	5.2
10	22 Jan 1928	38.600	22.600	5.4
11	22 Apr 1928	37.900	23.000	5.2
12	22 Apr 1928	38.070	22.820	6.3
13	25 Apr 1928	38.000	23.000	5.2
14	29 Apr 1928	38.000	23.000	5.2
15	4 Jan 1931	37.900	22.900	5.6
16	25 Mar 1931	38.500	22.200	5.3
17	16 Apr 1947	38.300	21.800	5.2
18	17 Jan 1948	38.300	21.500	5.2
19	13 Jun 1953	38.100	22.600	5.5
20	5 Sep 1953	37.900	23.100	5.8
21	30 Nov 1953	38.500	21.400	5.2
22	17 Apr 1954	38.000	22.800	5.3
23	19 Jan 1962	38.300	21.900	5.3
24	19 Jan 1962	38.100	22.100	5.3
25	4 Oct 1962	37.900	22.300	5.2
26	6 Jul 1965	38.270	22.300	6.3
27	4 Jan 1967	38.400	22.000	5.5
28	8 Jun 1968	38.300	22.900	5.2
29	8 Apr 1970	38.360	22.530	6.2
30	20 Apr 1970	38.240	22.650	5.4
31	1 Oct 1970	38.090	22.730	5.2
32	14 Nov 1974	38.500	23.090	5.2
33	8 Jan 1975	38.160	22.790	5.5
34	4 Apr 1975	38.210	22.160	5.5
35	30 Jun 1975	38.500	21.640	5.7
36	21 Dec 1975	38.420	21.710	5.5
37	31 Dec 1975	38.486	21.661	6.0
38	24 Feb 1981	38.153	22.961	6.7
39	24 Feb 1981	38.162	23.080	5.2
40	25 Feb 1981	38.083	23.139	6.4
41	4 Mar 1981	38.204	23.236	6.3
42	5 Mar 1981	38.216	23.148	5.4
43	7 Mar 1981	38.198	23.269	5.4
44	11 Feb 1984	38.369	22.091	5.6
45	7 Jun 1989	38.000	21.630	5.2
46	30 May 1992	37.930	21.440	5.2
47	18 Nov 1992	38.340	22.440	5.9
48	14 Jul 1993	38.170	21.770	5.6
49	4 Nov 1993	38.370	22.050	5.3
50	15 Jun 1995	38.362	22.200	6.5
51	15 Jun 1995	38.308	22.111	5.7
52	5 Nov 1997	38.395	22.452	5.3
53	10 Apr 2007	38.551	21.636	5.3
54	10 Apr 2007	38.529	21.532	5.3
55	10 Apr 2007	38.551	21.642	5.3
56	5 Jun 2007	38.542	21.654	5.4
57	4 Feb 2008	38.101	21.985	5.5
58	4 Feb 2008	38.088	21.949	5.2
59	8 Jan 2008	37.952	21.537	6.4
60	18 Jan 2010	38.404	21.961	5.5
61	22 Jan 2010	38.432	22.007	5.4

$M \geq 6.2$, and one event of $M = 5.7$ associated with a smaller fault along the sequence of faults that bound the south coastline, which occurred in the study area during the instrumental era (Table 2). The change in Coulomb failure function, ΔCFF, is computed in order to quantify the closeness to failure of the subsequent earthquakes at their locations. It depends on shear stress change $\Delta\tau$ (computed in the slip direction) and fault-normal stress change $\Delta\sigma$ (positive for extension). It takes the form

$\Delta CFF = \Delta\tau + \mu' \cdot \Delta\sigma$where μ' stands for the apparent friction coefficient.

The shear modulus and Poisson's ratio are fixed at 3.3×10^5 bar and 0.25, respectively in the calculations, based on previous laboratory experiments and studies. We refer to previous results in order to select the appropriate value of the apparent friction coefficient μ' (Papadimitriou, 2002; Karakostas et al., 2014). Thorough discussion has been made by Deng and Sykes (1997), who have tested various values for μ' and concluded that the results are not very sensitive when it changes. In our case a value of $\mu' = 0.4$ is considered to be suitable (Console et al., 2013). The spatial distribution of ΔCFF provides evidence on whether an earthquake was brought closer to, or moved farther from failure. A positive value of ΔCFF for a particular fault exhibits an increased likelihood of fault rupture.

Calculations of the static Coulomb stress changes ΔCFF are not trivial and require knowledge of the fault mechanisms and the slip distribution onto them. The Corinth Gulf Fault System is well studied and thus it makes it possible to extract the necessary geological and geodetic information. The majority of the focal mechanisms indicate normal faulting (Jackson, 1987; Hatzfeld et al., 1996; Bernard et al., 1997), a fact that is also apparent in microearthquake mechanisms (Hatzfeld et al., 2000; Rigo et al., 1996; Mesimeri et al., 2016). Table 2 lists the fault segments associated with the events used in our calculations and gives information on their geometry parameters and the coseismic slip along with the respective references (Jackson et al., 1982; Hatzfeld et al., 1996; Bernard et al., 1997; Console et al., 2013).

The events used in our computations of static Coulomb stress changes (Table 2) are assumed to be characteristic since earthquakes in the Corinth Gulf area with magnitudes $\sim M_w 6.0$ completely rupture the brittle crustal layer, which is one of the main assumptions of the characteristic earthquake hypothesis. Among the causative sources we have considered not only the eight major faults along the south coastline of the rift but also the Kapareli fault which is associated with the third event of the 1981 sequence, the $M_w 6.3$ event of the 4th March 1981 (Hubert et al., 1996; Console et al., 2013).

Fig. 3 shows the coseismic stress changes associated with the events presented in Table 2. We aim to figure out how an event that occurs in one part of the Gulf affects earthquake occurrence in the other part, i.e., if the relative segments get closer to or farther from failure due to the stress transfer from the causative fault. The epicenters of the eight characteristic earthquakes are depicted by red stars and the associated fault segments are traced in white colour. The yellow circles represent the events with $M \geq 5.2$ that occurred in the eastern part until the occurrence of the next characteristic earthquake and the red diamonds the corresponding events of the western part. Fig. 3a shows the Coulomb stress changes due to the coseismic slip of the 22 April 1928, $M = 6.3$ earthquake. The event is associated with the Offshore Perachora fault located at the eastern part of the Corinth Gulf. We are interested in the values of ΔCFF at the locations of the events occurring from 1928 to 1965, the occurrence year of the next characteristic event. We focus particularly on the events occurring in the western part for extracting information on the kind of interactions. Six out of thirteen events of this time interval occurred in the western part and all of them inside stress enhanced areas, which implies possible triggering.

Following the same line of thought, we proceeded with the subsequent characteristic events. Fig. 3b shows the Coulomb stress changes due to the coseismic slip of the 6 July 1965 event, which is associated with the Eliki fault segment located in the western part. We may see that during the time interval between this characteristic event and the next one occurring in 8 April 1970, one event, with positive ΔCFF value occurred in the eastern part. Similar interpretations for the rest of the events referred in Table 2 leads to the results presented in Table 3.

Fig. 4 depicts histograms of the number of events that occurred in both subareas as a function of the ΔCFF value at their locations. The prevailing number of earthquakes located inside areas of positive ΔCFF values indicates that fault segments belonging to the western part get

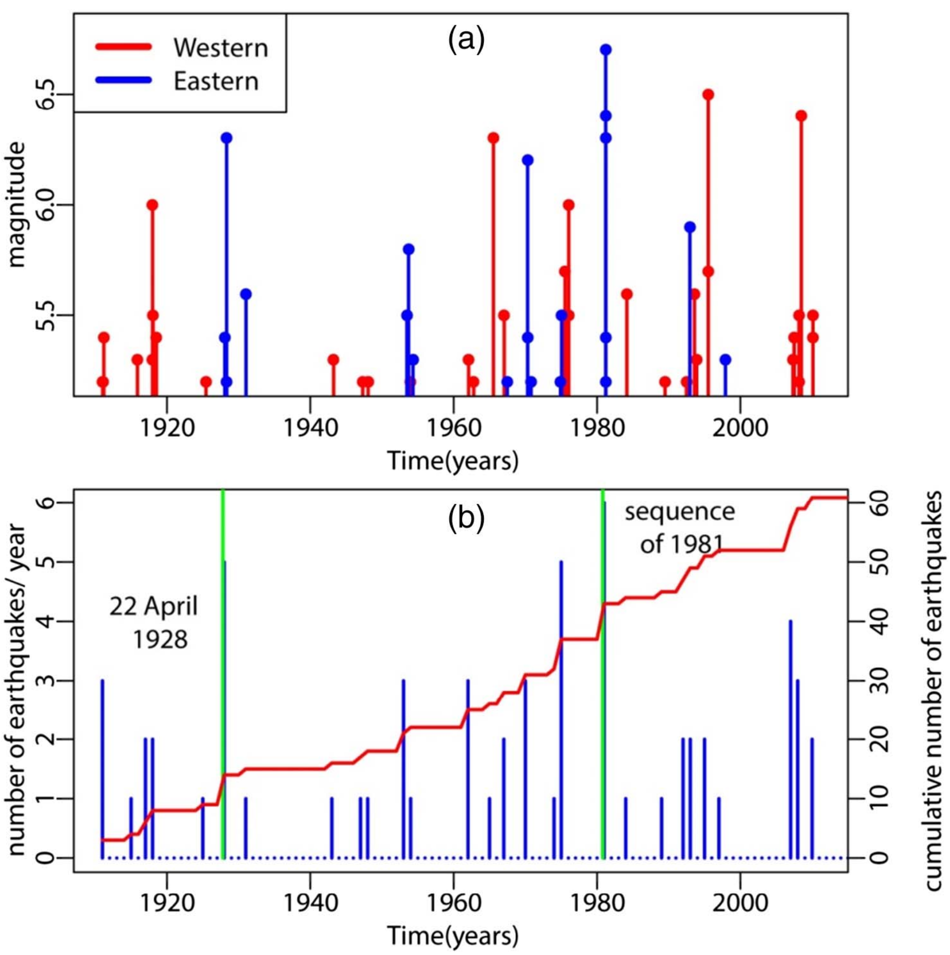

Fig. 2. (a) Temporal distribution of earthquakes with M ≥ 5.2 that occurred in the study area from 1911 to 2016.
(b). Frequency (left axis) and cumulative number of events (right axis) versus time (in years). The green lines show two cases of characteristic earthquakes that provoked a large number of events. (For interpretation of the references to colour in this figure legend, the reader is referred to the web version of this article.)

Table 2
Rupture models for the earthquakes included in the stress calculation model.

Date	Time	Lat.	Long.	L (km)	Slip (m)	M_w	Fault segment	Focal mechanism			Part	Ref
								Strike	Dip	Rake		
1928, April 22	20:13:46	38.07	22.82	18	0.54	6.3	Offshore Perachora	275	40	− 80	eastern	1
1965, July 6	03:18:42	38.27	22.30	12	0.351	6.3	Eliki	281	34	− 71	western	1
1970, April 8	13:50:28	38.36	22.53	12	0.19	6.2	Xylokastro	265	30	− 81	eastern	1
1981, February 24	20:53:37	38.153	22.961	19	1.3	6.7	Skinos	264	42	− 80	eastern	2
1981, February 25	02:35:51	38.083	23.139	13	0.66	6.4	Alepochori	241	44	− 85	eastern	2
1981, March 4	21:58:05	38.204	23.236	13	0.34	6.3	Kapareli	50	45	− 90	eastern	3
1992, November 18	21:10:42	38.340	22.440	8	0.19	5.7	Offshore Akrata	270	30	− 81	eastern	4
1995, June 15	00:15:50	38.362	22.200	16	0.87	6.4	Aigion	277	33	− 77	western	5

(1) Console et al. (2013), (2) Jackson et al. (1982), (3) Hubert et al. (1996), (4) Hatzfeld et al. (1996), (5) Bernard et al. (1997)

closer to failure due to earthquakes occurring in the eastern part. On the contrary, there is not strong evidence provided by the observations that earthquakes occurring in the western part affect the earthquake occurrence in the eastern part of the Corinth Gulf. The sample size on which we are based for concluding about the kind of interactions among the two subareas may be considered limited. Independently of the size, however, the pattern is persistent and the same in all cases. It is reasonable to state that since it concerns along strike positioned normal faults, each failure encourages the activation of the adjacent segments.

Calculations of Coulomb stress variations in the SRM have been introduced by Jiang et al. (2011). They proposed a Multi-dimensional Stress Release Model (MSRM), a statistical model for describing the evolution of seismicity in space, time and magnitude. The extension to spatial dimensions was accomplished by including a coseismic stress transfer model in the SRM. The MSRM deals with the interactions among earthquakes in the sense that it can yield the map of earthquake rates at any time. On the contrary, in the LSRM the whole area is divided in subareas trying to find out the connection between larger parts with similar tectonic features.

4. Formulation and application of the stress release model (SRM)

4.1. Formulation of the LSRM

In the Stress Release Model the probability for an earthquake occurrence depends on an unobserved quantity $X(t)$ that represents the stress level in an area changing over time Vere-Jones and Deng (1988). Starting from an initial stress level $X(0)$ it is increased linearly between two consecutive earthquakes based upon the assumption that the strain energy is accumulated due to constant tectonic loading and drops

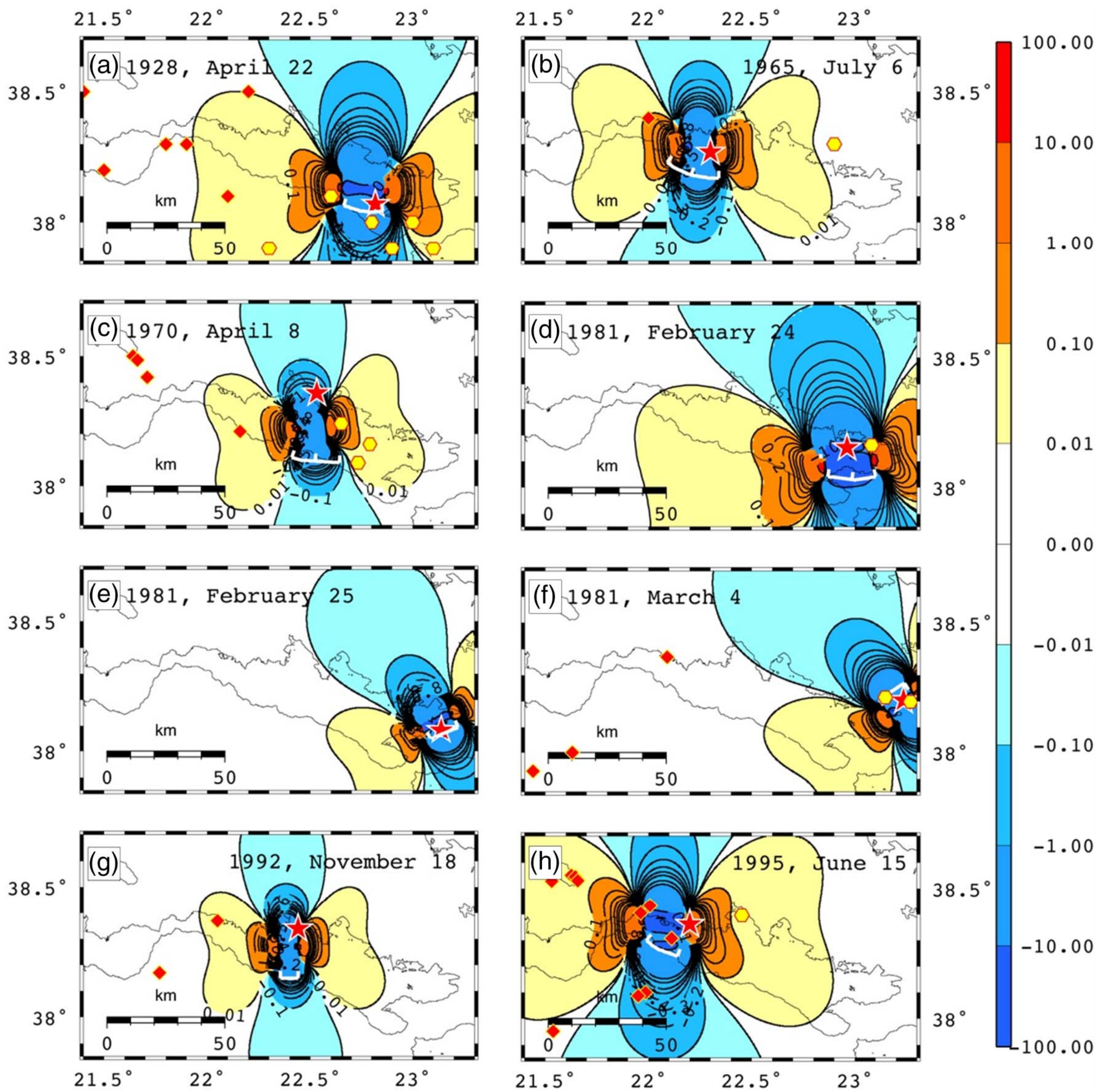

Fig. 3. Coulomb stress changes due to the coseismic slip of the characteristic events (stars) presented in Table 1. Coulomb stress is calculated for normal faults at a depth of 8.0 km. Changes are denoted by the colour scale at the right (in bars). The epicenters of the characteristic events are depicted by the red stars. Earthquakes that occurred in the western part of the Corinth Gulf are represented with red diamonds and those that occurred in the eastern part with yellow hexagons. The associated fault segments are traced in white colour. (For interpretation of the references to colour in this figure legend, the reader is referred to the web version of this article.)

Table 3
Number of events that occurred in areas of positive and negative ΔCFF values due to the coseismic slip of the characteristic events in the two subareas of the Corinth Gulf.

To	West		East	
From	Positive ΔCFF	Negative ΔCFF	Positive ΔCFF	Negative ΔCFF
West	7	4	2	0
East	14	1	9	5

suddenly as it is released when an earthquake occurs. The stress level can thus be written

$$X(t) = X(0) + \rho t - S(t),$$

where $X(0)$ stands for the stress level at the starting time, ρ is the constant loading rate and $S(t)$ is the accumulated stress release due to earthquakes in the study area over the period $(0, t)$, that is,

$$S(t) = \sum_{t_i<t} S_i$$

where t_i, S_i are the origin time and the stress release, respectively, associated with the i-th earthquake.

For the model application, the stress is calculated from the earthquake magnitude, and for this reason an appropriate relationship is seeking between the earthquake magnitude and the stress variation. According to Bufe and Varnes (1993) a measure of the total energy released during an earthquake is expressed by the cumulative Benioff's strain. Thus, the stress released by the i-th earthquake takes the form

$$S_i = 10^{0.75(M_i - M_{th})},$$

where M_i is the earthquake magnitude and M_{th} the smallest magnitude in the dataset (Kanamori and Anderson, 1975).

The stress level is then translated into hazard. The stochastic behavior of the point process is described by the conditional intensity function $\lambda*(t)$, which is the instantaneous occurrence probability (Daley and Vere-Jones, 2003). It is usually assumed to have an exponential form

$$\lambda^*(t) = \Psi(X(t)) = \exp\{\mu + \nu[X(0) + \rho t - S(t)]\}$$
$$= \exp\{a + b[t - cS(t)]\},$$

where a, b and c are parameters to be estimated.

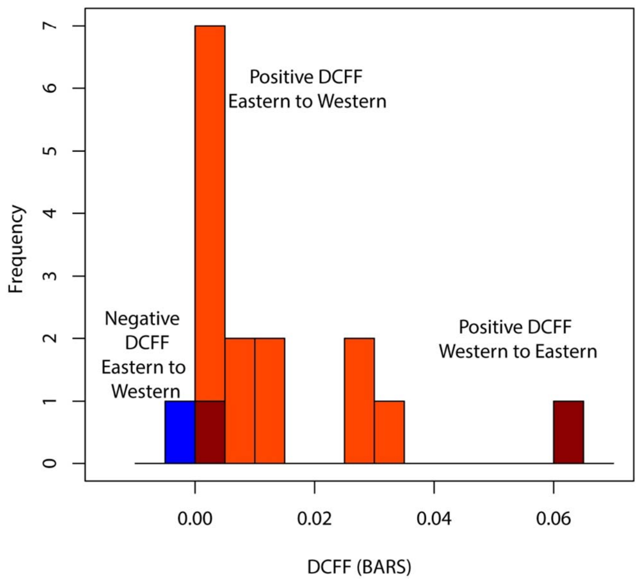

Fig. 4. Overlapping histogram showing the number and kind of interactions between the two parts of the Corinth Gulf.

The Simple Stress Release Model takes into account only the effect of the stress level change in the same area. In practice though, the seismicity of an area is also influenced by the seismicity and the stress change perturbations of the surrounding area. As a first step, Zheng and Vere-Jones (1994) concluded that dividing a large area into subareas can improve the fit. Liu et al. (1998) did not just subdivide the study area, but they incorporated interactions between different subareas. The model was enriched, thus leading to the Linked Stress Release Model (LSRM). The evolution of stress $X_i(t)$ in each subarea i can be written

$$X_i(t) = X_i(0) + \rho_i t - \sum_j \theta_{ij} S(t,j),$$

where $S(t, j)$ stands for the accumulated stress in the j subarea for the time interval (0,t) and the coefficient θ_{ij} measures the ratio of stress release which is transferred to the subarea i due to an earthquake occurring in the subarea j. The coefficient θ_{ii} is set to be equal to 1, since we assume that the occurrence of an earthquake causes the release of a significant amount of the accumulated energy. This means that when an earthquake occurs in a subarea, in that site it became stress free and its hazard in that site is decreased. The parameters θ_{ij} may take either positive or negative values revealing the kind of interaction. A positive value would mean that the earthquake in one subarea provokes damping in the adjacent subarea whereas a negative value of θ_{ij} implies excitation.

For proceeding to the application it is necessary to describe how the point process behaves. The conditional intensity function (c.i.f.) for each subarea i usually takes the form

$$\lambda_i^*(t) = \Psi(X_i(t)) = \exp\left\{a_i + \nu_i\left[\rho_i t - \sum_j \theta_{ij} S(t,j)\right]\right\},$$

where a_i, ν_i, ρ_i and θ_{ij} are the parameters to be estimated. Following the parameterization of Liu et al. (1998) and setting $b_i = \nu_i\rho_i$ and $c_{ij} = \theta_{ij} / \rho_i$, the c.i.f. can be written

$$\lambda_i^*(t) = \exp\left\{a_i + b_i\left[t - \sum_j c_{ij} S(t,j)\right]\right\},$$

where a_i, b_i and c_{ij} are the parameters to be estimated.

The estimation is performed numerically by maximizing the log-likelihood function. Restrictions should be set so that the physical meaning of the process to be taken into account. Since the loading rate ρ_i and the parameter ν_i, which depends on the heterogeneity and the strength of the crust in the study area, take only positive values, the parameters b_i and $c_{ii} = 1 / \rho_i$ should be positive. On the contrary, the transfer parameters c_{ij} take positive values if the interactions are inhibitory or negative values if they are excitatory.

4.2. Application of the LSRM in the Corinth Gulf

The aim of the stochastic modeling is the combination of the mathematical tools with the geophysical meaning. The application of the LSRM is performed under restrictions here for the physical meaning of the process to be taken into account. This is actually the difference with the approach of Mangira et al. (2017), namely to constrain the values of the transfer parameters and impose some rules that control the interaction between the western and eastern part of the study area. The use of the Coulomb stress changes provided insight to the style of this interaction that would reflect the physical process. As mentioned in the previous section, earthquakes occurring in the eastern part tend to increase the seismicity of the western part, while they occur independently from the earthquakes of the western part. The additional restrictions for the transfer parameters is to set the parameter c_{12} to be negative and the parameter c_{21} equal to 0, since the interaction from the western part is not significant.

The estimation of the parameters was performed numerically by means of a quasi–Newton method, the Broyden–Fletcher–Goldfarb–Shanno (BFGS) method. Each positive parameter is transformed and reparametrized as an exponential function of a parameter lying on the real line. The optimization algorithm led to successful convergence and the final solution obeys the aforementioned restrictions. The standard errors were calculated using the Fisher information matrix. The technique requires evaluation of second derivatives of the log likelihood. This is actually a way of measuring how much information is provided by the estimated parameters. This information measure can then be used to find bounds on the variance of estimators. The confidence intervals are constructed by the asymptotic normality of the MLE, obtained according to the central limit theorem under a large size of the sample. Table 4 gives information on the values of the estimated parameters, the corresponding standard errors and the 90% confidence intervals. The maximum value of the log-likelihood function is found equal to − 135.4984.

Fig. 5a and b show the conditional intensity functions for the western and eastern part of the Corinth Gulf, respectively. The temporal distribution for the earthquakes with M ≥ 5.2 that occurred from 1911 to 2016 is also shown. The green line represents the mean occurrence level of the Poisson model. We may notice in Fig. 5b that, as expected, earthquakes occurring in the western part of the Corinth Gulf, do not affect the seismic activity in the eastern part, since the curve of the c.i.f. drops only when an event occurs in the eastern part and not in the western part.

A comparison is worth to be made between Mangira et al. (2017) and the current article since the study area is the same and the model was applied with and without restrictions concerning the transfer parameters. The two datasets though are slightly different. The

Table 4
Restricted LSRM's estimated parameters, standard errors and 90% confidence intervals.

Parameter	Estimate	Standard error	90% Confidence interval
$a1$	− 1.6602	0.4025	(− 2.3223, − 0.9981)
$a2$	− 1.7419	0.5073	(− 2.5765, − 0.9074)
$b1$	0.0400	0.3513	(0.0224, 0.0713)
$b2$	0.0190	1.0669	(0.0033, 0.1098)
$c11$	1.5647	0.2546	(1.0292, 2.3787)
$c12$	− 0.2858	1.0237	(− 1.5394, − 0.0530)
$c22$	1.3876	0.3796	(0.7431, 2.5911)

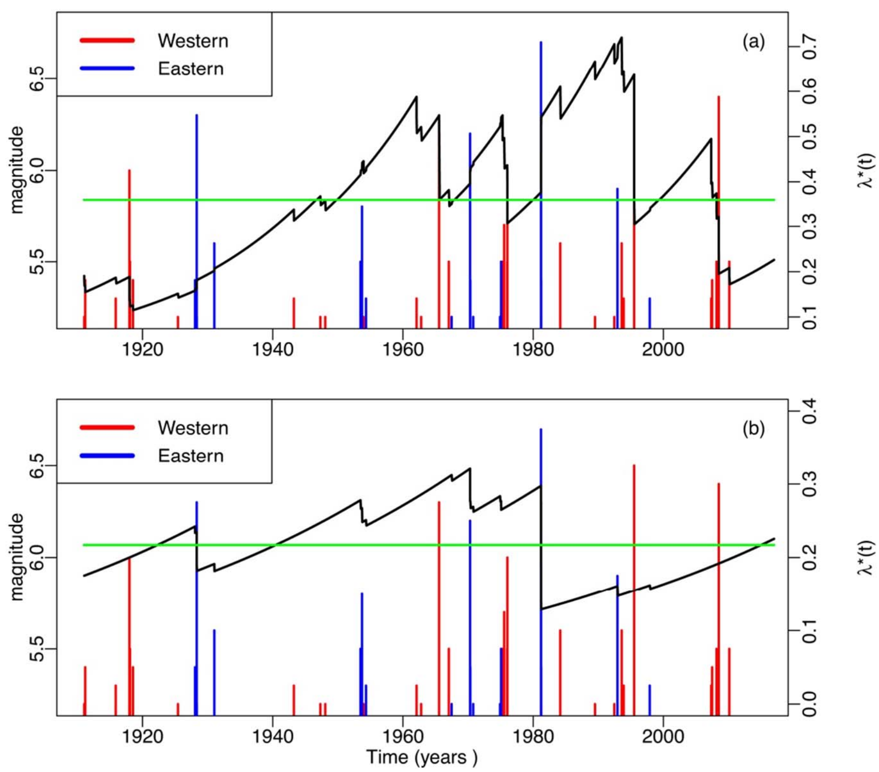

Fig. 5. Conditional intensity functions versus time for each subarea of the Corinth Gulf, when applying the Restricted LSRM. a Western part. b Eastern part. The green line represents the mean occurrence level of the Poisson model. (For interpretation of the references to colour in this figure legend, the reader is referred to the web version of this article.)

difference is due to the partition between the two subareas. In general, the regionalization and the identification of the appropriate subareas is a matter of major importance in the LSRM. In this study the boundaries between them were strictly set at the edges of the major faults bounding the southern coastline. This results to the slight modifications of the respective datasets by two earthquakes. Thus, the division was slightly changed so that each fault segment belongs completely in only one subarea. One of the events that were moved from the eastern to the western part is the strong earthquake of 1965 with M_w6.3. It was then intriguing to check if the application of the LSRM would give different results, particularly since the interaction from east to west is quite weak.

According to the new computations, the parameter c_{12} was found negative (the 90% confidence interval contains also positive values) and the parameter c_{21} was found positive; negative values are also contained in the confidence interval, not excluding the value of 0 (Table 5). We may see that the new results are not opposed to positive Coulomb stress changes in the along strike normal faults. In the restricted model, however, the constraints are more rigorous since the parameter c_{12} is purely negative and the parameter c_{21} is equal to zero. The conditional intensity functions versus time for the western and eastern part are presented in Fig. 6a and b respectively.

For evaluating the performance of the competing models, a comparison between the LSRM and the restricted LSRM can be made by

Table 5
LSRM's estimated parameters, standard errors and 90% confidence intervals.

Parameter	Estimate	Standard error	90% confidence interval
$a1$	− 1.2059	0.3851	(− 1.8395, − 0.5723)
$a2$	− 1.7580	0.5507	(− 2.6639, − 0.8521)
$b1$	0.0072	2.3139	(0.0002, 0.3275)
$b2$	0.0329	0.7625	(0.0093, 0.1154)
$c11$	2.6381	2.0231	(0.0946, 73.5635)
$c12$	− 1.6504	5.6775	(− 10.9899, 7.6891)
$c21$	1.0650	0.9467	(− 0.4924, 2.6224)
$c22$	0.4614	1.6014	(0.0331, 6.4296)

means of the Akaike Information Criterion. In the first case, the value of the AIC is found equal to 282.63 while according to the present computations it is equal to 284.99. In the latter case the AIC value is higher, which means that the Akaike Information Criterion favors the use of the LSRM. The assumptions we made based on the pattern derived from the Coulomb stress change computations are not opposing though, but rather confirm the results.

4.3. Application of the LSRM to synthetic earthquake catalog

As previously mentioned Console et al. (2015) developed an earthquake simulator algorithm in order to model the seismic activity of the study area. The earthquake simulator is based on physics trying to reproduce the long-term seismicity of a relatively simple fault system, where each seismogenic source is represented as a rectangle consisting of a number of cells. The initial state of stress in each cell is assumed to be close to the threshold. When a cell is ruptured, the surrounding cells may also rupture due to Coulomb stress changes. Particular attention has been given in imposing the conditions of initiating and then stopping a rupture. As it regards the Corinth Gulf, based on seventeen characteristic events that occurred since 1714, Console et al. (2015) created a synthetic catalog which contains 500,000 events in a period of 100,000 years. In the simulation algorithm an average slip rate released by earthquakes for every single segment is imposed combining geological and geodetic information, considering interaction between earthquake sources and taking into account the effect of minor earthquakes in redistributing stress. The simulator can replicate real features of the observed seismicity including time, space and magnitude behavior.

Even in areas with adequate seismic monitoring, like the study area, seismic catalogs are short compared with the underlying process. Therefore, the simulated catalog of Console et al. (2015) was an excellent opportunity to check if the stress release model successfully fits the earthquake occurrence. The synthetic catalog was actually created based on some assumptions, with one of its basic ingredients is the elastic rebound theory of Reid. The LSRM is also constructed upon the

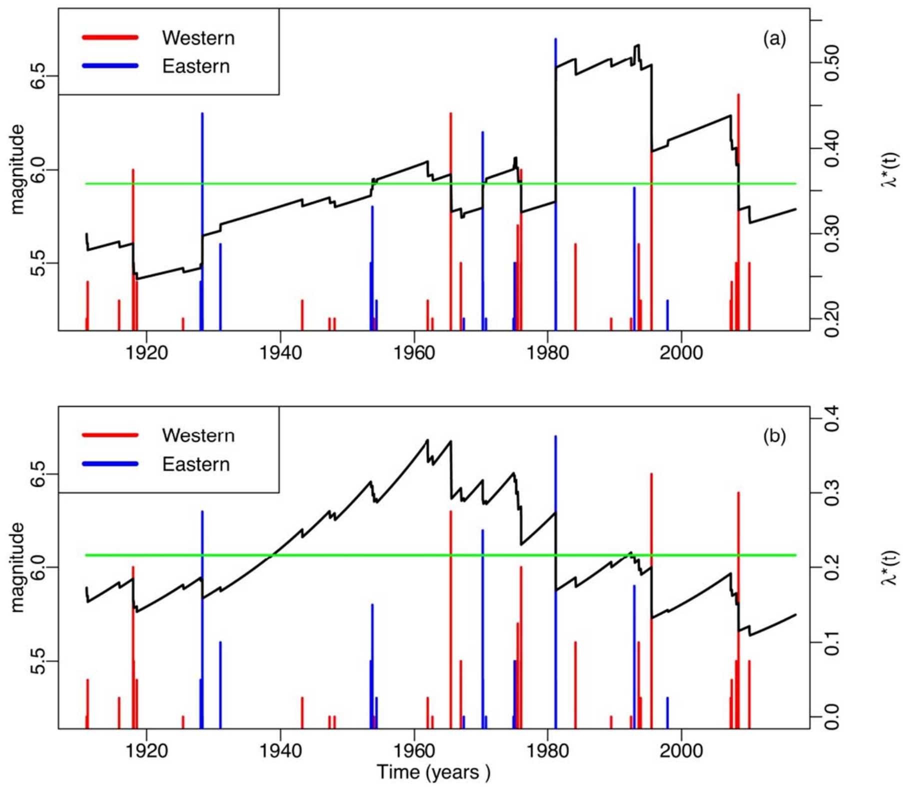

Fig. 6. Conditional intensity functions versus time for each subarea of the Corinth Gulf, when applying the LSRM without constraints. a Western part. b Eastern part. The green line represents the mean occurrence level of the Poisson model. (For interpretation of the references to colour in this figure legend, the reader is referred to the web version of this article.)

elastic rebound theory. The simulator applies the elastic rebound theory to a very large number of cells of 1 km × 1 km size, and includes a physical model of Coulomb stress transfer, while the LSRM considers only two larger parts of the study area without inclusion of a physical model for stress transfer. As the focal mechanism of the faults in the Corinth Gulf is predominantly normal, the simulator applies the Coulomb stress transfer simmetrically in both ways along the strike of the fault. The interaction is much stronger close to the rupturing faults than far from them. So, it is possible that faults far apart in the two different areas have very little interaction, while the LSRM treats all the earthquakes in the same way in each of the two study areas.

Regardless the initial hypotheses, the synthetic catalog of Console et al. (2015) simulates the earthquake generation at a certain study area. Therefore, the LSRM was applied for a full exploitation of a dataset going back in time using many different samples. We applied the LSRM in several periods of 1000 years duration using the same restrictions derived from the Coulomb stress changes and with the same magnitude threshold, i.e., $M_{th} = 5.2$. The parameter c_{21} is set to be zero meaning that earthquakes occurring in the western part do not affect the earthquake occurrence in the eastern part and the parameter c_{12} is restricted to be negative assuming excitatory behavior.

Table 6 gives information on the estimated parameters for 8 different periods lasting 1000 years each. The corresponding c.i.f. are shown in Fig. 7. The standard errors of the estimated parameters derived from the synthetic catalogs are much smaller than those of the real one due to the large sample size. Parameters a and b are quite similar in both applications. Parameters c_{11} and c_{22} are systematically larger when the model is applied to the synthetic catalogs rather than to the real one. This discrepancy is not dramatic, taking into account the uncertainty in the slip rate adopted in the model of the simulator, which is proportional to the occurrence rate, assuming that all accumulated strain is released by earthquakes. We may also notice that the transfer parameter c_{12} of the simulated data is closer to zero than the one derived from the real data, a fact that certainly derives from the constraint imposed.

5. Discussion and concluding remarks

The LSRM is applied to fit data from the Corinth Gulf, one of the most active areas in the Aegean, which accommodates several moderate to strong earthquakes. It implies an exponentially increasing conditional intensity function between earthquakes and a sudden reduction when an event occurs. By incorporating information provided from the calculation of Coulomb stress changes due to the coseismic slip of the strongest earthquakes during the study period, we propose a restricted stress release model where the western part of the Corinth Gulf is excited due to earthquakes occurring in the eastern part while the eastern part is not affected by earthquakes occurring in the western part.

Table 6
Estimated parameters for 8 data samples each covering a period of 1000 years.

	12,000–13,000	15,000–16,000	22,000–23,000	36,000–37,000	47,000–48,000	66,000–67,000	90,000–91,000	99,000–100,000
$a1$	− 4.319	− 1.858	− 3.564	− 2.755	− 2.504	− 2.868	− 0.927	− 1.606
$a2$	− 2.437	− 4.565	− 1.596	− 2.708	− 1.463	− 1.547	− 4.420	− 2.870
$b1$	0.046	0.023	0.072	0.052	0.030	0.024	0.017	0.017
$b2$	0.043	0.039	0.065	0.020	0.046	0.018	0.027	0.024
$c11$	3.108	2.658	3.063	3.288	3.199	2.549	3.067	3.108
$c12$	− 0.007	− 0.033	− 0.015	− 0.274	− 0.094	− 0.018	− 0.018	− 0.008
$c22$	3.716	3.952	3.546	4.046	3.867	4.182	4.064	3.905

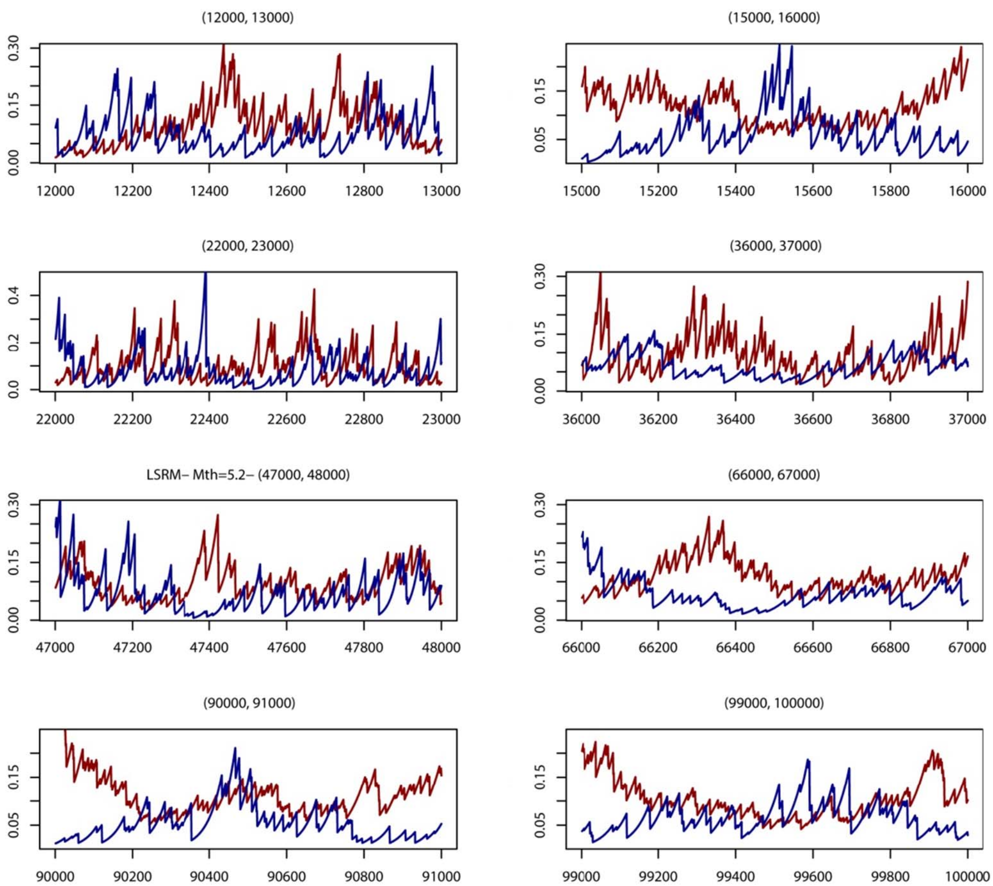

Fig. 7. Conditional intensity functions versus time for the simulated data with Mth = 5.2 for several periods of 1000 years. The red curves refer to the western part of the Corinth Gulf and the blue ones to the eastern part. (For interpretation of the references to colour in this figure legend, the reader is referred to the web version of this article.)

These restrictions are used in order to apply the LSRM to synthetic earthquake catalogs that simulate the seismic activity. It is noteworthy that during the current investigation the analysis was also performed without constraints. In most of the cases examined, the transfer parameters c_{12} and c_{21} were found positive with very few negative values. This result could be ascribed to the above mentioned symmetry of the Coulomb stress transfer and to the short distance range of the main interaction between faults.

The different results derived with and without constraints indicate that, as expected, the constraints determine the final solution. This means that for the model application the appropriate restrictions that take into account the physical meaning of the process may influence the outcome. In our case, the coseismic stress transfer model gives insight regarding the transfer parameters. Conversely, we should very carefully impose restrictions for the results to be reliable.

We carefully put care in avoiding possible computational issues, since a disadvantage of the maximum likelihood estimation (MLE) method is the fact that it is sensitive to the selection of the initial points. The parameter space was scanned very carefully by means of a dense grid and a large number of initial values were tested. We conclude thus that we achieved adequate convergence by thoroughly investigating the maximum of the log-likelihood function.

The sensitivity of the model to the regionalization is also highlighted. The importance of the determination of the appropriate subareas is confirmed by applying the LSRM in two slightly different datasets, the one used by Mangira et al. (2017) and the one in the present work. Only two events, located to the boundary between the two subareas, are now assumed to belong to the eastern rather than the western part resulting in different kind of interactions between the two subareas. This fact indicates that we should cautiously identify the different subareas by using known tectonic features, such as the seismicity rate and the boundaries of the faults.

Acknowledgments

The constructive comments of two reviewers are acknowledged for their contribution to the improvement of the paper. Gratitude is also extended to Prof. Wang for his editorial assistance and constructive suggestions. The authors would like to express their sincere appreciation to Prof. G. Tsaklidis for critically reading the manuscript and making valuable suggestions. The stress tensors were calculated using a program written by J. Deng (Deng and Sykes, 1997), based on the DIS3D code of S. Dunbar, which later improved (Erickson, 1986) and the expressions of G. Converse. The software Generic Mapping Tools was used to plot some figures (Wessel and Smith, 1998). Geophysics Department Contribution 906.

References

Armijo, R., Meyer, B., King, G.C.P., Rigo, A., Papanastassiou, D., 1996. Quaternary evolution of the Corinth rift and its implications for the Late Cenozoic evolution of the Aegean. Geophys. J. Int. 126, 11–53.

Bebbington, M., Harte, D., 2001. On the statistics of the linked stress release process. J. Appl. Probab. 38, 176–187.

Bebbington, M., Harte, D., 2003. The linked stress release model for spatio-temporal seismicity: formulations, procedures and applications. Geophys. J. Int. 154, 925–946.

Bernard, P., Briole, P., Meyer, B., Lyon-Caen, H., Gomez, M., Tiberi, C., Berge, C., Cattin, R., Hatzfeld, D., Lachet, C., Lebrun, B., Dechamps, A., Courbouleux, F., Larroque, C., Rigo, A., Massonnet, D., Papadimitriou, P., Kassaras, J., Diagourtas, D., Makropoulos, K., Veis, G., Papazisi, E., Mitsakaki, C., Karakostas, V., Papadimitriou, E., Papanastasiou, D., Chouliaaras, M., Stavrakakis, D., 1997. The Ms = 6.2, June 15, 1995 Aigion earthquake (Greece): evidence for low angle normal faulting in the Corinth rift. J. Seismol. 1, 131–150.

Bufe, C., Varnes, D., 1993. Predictive modeling of the seismic cycle of the greater San Francisco Bay region. J. Geophys. Res. 98, 9871–9883.

Cocco, M., Rice, J.R., 2002. Pore pressure and poroelasticity effects in Coulomb stress analysis of earthquake interactions. J. Geophys. Res. 107. http://dx.doi.org/10.1029/2000JB000138.

Console, R., Falcone, G., Karakostas, V., Murru, M., Papadimitriou, E., Rhoades, D., 2013. Renewal models and coseismic stress transfer in the Corinth Gulf, Greece, fault

system. J. Geophys. Res. 118, 3655–3673.
Console, R., Carluccio, R., Papadimitriou, E., Karakostas, V., 2015. Synthetic earthquake catalogs simulating seismic activity in the Corinth Gulf, Greece, fault system. J. Geophys. Res. 120, 326–343.
Daley, D., Vere-Jones, D., 2003. An Introduction to the Theory of Point Processes, 2nd edition. Vol. 1. Springer, New York, pp. 211–287.
Deng, J., Sykes, L.R., 1997. Evolution of the stress field in southern California and triggering of moderate-size earthquakes: a 200-year perspective. J. Geophys. Res. 102, 9859–9886.
Erickson, L., 1986. User's Manual for DIS3D: A Three-dimensional Dislocation Program With Applications to Faulting in the Earth. Master's thesis. Stanford Univ (167 pp).
Gomberg, J., Belardinelli, M.E., Cocco, M., Reasenberg, P., 2005. Time-dependent earthquake probabilities. J. Geophys. Res. 110. http://dx.doi.org/10.1029/2004JB003405.
Hardebeck, J.L., 2004. Stress triggering and earthquake probability estimates. J. Geophys. Res. 109. http://dx.doi.org/10.1029/2003JB002437.
Hatzfeld, D., Karakostas, V., Ziazia, M., Kassaras, I., Papadimitriou, E., Makropoulos, K., Voulgaris, N., Papaioannou, C., 1996. The Galaxidi earthquake of 18 November 1992; a possible asperity within normal fault system of the Gulf of Corinth (Greece). Bull. Seismol. Soc. Am. 86 (6), 1987–1991.
Hatzfeld, D., Karakostas, V., Ziazia, M., Kassaras, I., Papadimitriou, E., Makropoulos, K., Voulgaris, N., Papaioannou, C., 2000. Microseismicity and faulting geometry in the Gulf of Corinth. Geophys. J. Int. 141, 438–456.
Hubert, A., King, G., Armijo, R., Meyer, B., Papanastassiou, D., 1996. Fault re–activation, stress interaction and rupture propagation of the 1981 Corinth earthquake sequence. Earth Planet. Sci. Lett. 142, 573–585.
Imoto, M., Hurukawa, N., 2006. Assessing potential seismic activity in Vrancea, Romania, using a stress-release model. Earth Planets Space 58, 1511–1514.
Jackson, J.A., 1987. Active continental deformation and regional metamorphism. Philos. Trans. R. Soc. Lond. A321, 47.
Jackson, J.A., White, N.J., 1989. Normal faulting in the upper continental crust: observations from regions of active extension. J. Struct. Geol. 11, 15–36.
Jackson, J., Cagnepain, A., Houseman, J.G., King, G.C.P., Papadimitriou, P., Soufleris, C., Virieux, J., 1982. Seismicity, normal faulting and the geomorphological development of the Gulf of Corinth (Greece): the Corinth earthquakes of February and March 1981. Earth Planet. Sci. Lett. 57, 377–397.
Jiang, M., Zhu, S., Chen, Y., Ai, Y., 2011. A new multidimensional stress release statistical model based on coseismic stress transfer. Geophys. J. Int. 187, 1479–1494.
Kanamori, H., Anderson, D.L., 1975. Theoretical basis of some empirical relations in seismology. Bull. Seismol. Soc. Am. 65 (5), 1073–1095.
Karakostas, V., Papadimitriou, E., Gospodinov, D., 2014. Modelling the 2013 North Aegean (Greece) seismic sequence: geometrical and frictional constraints, and aftershock probabilities. Geophys. J. Int. 197, 525–541.
King, G.C.P., Cocco, M., 2001. Fault interaction by elastic stress changes: new clues from earthquake sequences. Adv. Geophys. 44, 1–38.
Kuehn, N.M., Hainzl, S., Scherbaum, F., 2008. Non-Poissonian earthquake occurrence in coupled stress release models and its effect on seismic hazard. Geophys. J. Int. 174, 649–658.
Liu, J., Vere-Jones, D., Ma, L., Shi, Y., Zhuang, J.C., 1998. The principal of coupled stress release model and its application. Acta Seismol. Sin. 11, 273–281.
Liu, C., Chen, Y., Shi, Y., Vere-Jones, D., 1999. Coupled stress release model for time-dependent seismicity. Pure Appl. Geophys. 155, 649–667.
Lu, C., Vere-Jones, D., 2000. Application of linked stress release model to historical earthquake data: comparison between two kinds of tectonic seismicity. Pure Appl. Geophys. 157, 2351–2364.
Lu, C., Harte, D., Bebbington, M., 1999. A linked stress release model for historical Japanese earthquakes: coupling among major seismic regions. Earth Planets Space 51, 907–916.
Mangira, O., Vasiliadis, G., Papadimitriou, E., 2017. Application of a linked stress release model in Corinth gulf and Central Ionian Islands (Greece). Acta Geophys. http://dx.doi.org/10.1007/s11600-017-0031-z.
Mesimeri, M., Karakostas, V., Papadimitriou, E., Tsaklidis, G., Tsapanos, T., 2016. Detailed microseismicity study in the area of Florina (Greece): evidence for fluid driven seismicity. Tectonophysics 694, 424–435.
Papadimitriou, E., 2002. Mode of strong earthquake recurrence in the Central Ionian Islands (Greece): possible triggering due to Coulomb stress changes generated by the occurrence of previous strong shocks. Bull. Seismol. Soc. Am. 92, 3293–3308.
Papazachos, B.C., Papazachou, C.C., 2003. The Earthquakes of Greece. Ziti Publications, Thessaloniki, Greece.
Parsons, T., 2005. Significance of stress transfer in time–dependent earthquake probability calculations. J. Geophys. Res. 109. http://dx.doi.org/10.1029/2004JB003190.
Permanent Regional Seismological Network, 1981. (operated by the Aristotle University of Thessaloniki). https://doi.org/10.7914/SN/HT.
Rigo, A., Lyon–Caen, H., Armijo, R., Deschamps, A., Hatzfeld, D., Makropoulos, K., Papadimitriou, P., Kassaras, I., 1996. Microseismicity study in the western part of the Gulf of Corinth (Greece): implications for large–scale normal faulting mechanisms. Geophys. J. Int. 126, 663–688.
Roberts, S., Jackson, J., 1991. Active normal faulting in central Greece: An overview. In: Roberts, A.M., Yielding, G., Freeman, B. (Eds.), The Geometry of Normal Faults. Geol. Soc. Lond. Spec. Publ. 56. pp. 125–142.
Rotondi, R., Varini, E., 2006. Bayesian analysis of marked stress release models for time-dependent hazard assessment in the western Gulf of Corinth. Tectonophysics 423, 107–113.
Steacy, S., Gomberg, J., Cocco, M., 2005. Introduction to special section: stress transfer, earthquake triggering, and time-dependent seismic hazard. J. Geophys. Res. 110. http://dx.doi.org/10.1029/2004JB003356.
Stein, R.S., 1999. The role of stress transfer in earthquake occurrence. Nature 402, 605–609.
Stein, R., Barka, A., Dieterich, J., 1997. Progressive failure on the North Anatolian fault since 1939 by earthquake stress triggering. Geophys. J. Int. 128, 594–604.
Varini, E., Rotondi, R., 2015. Probability distribution of the waiting time in the stress release model: the Gompertz distribution. Environ. Ecol. Stat. 22, 493–511.
Varini, E., Rotondi, R., Basili, R., Barba, S., 2016. Stress release models and proxy measures of earthquake size. Application to Italian seismogenic sources. Tectonophysics 682, 147–168.
Vere-Jones, D., 1978. Earthquake prediction—a statistician's view. J Phys Earth 26, 129–146.
Vere-Jones, D., Deng, Y.L., 1988. A point process analysis of historical earthquakes from North China. Earthq. Res. China 2, 165–181.
Vere-Jones, D., Ben-Zion, Y., Zuniga, R., 2005. Statistical seismology. Pure Appl. Geophys. 162, 1023–1026.
Votsi, I., Tsaklidis, G., Papadimitriou, E., 2011. Seismic hazard assessment in Central Ionian Islands area based on stress release models. Acta. Geophysica 59, 701–727.
Wessel, P., Smith, W.H.F., 1998. New, improved version of the generic mapping tools released. Trans. Am. Geophys. Union 79, 579.
Zheng, X., Vere-Jones, D., 1994. Further applications of the stochastic stress release model to historical earthquake data. Tectonophysics 229, 101–121.